Pan-cancer analysis of pyrimidine metabolism reveal signaling pathways connections with chemoresistance role

Vignesh Ramesh[1,2#], Mert Demirdizen[1,3#], Luisa Pinna[1], Thomas Koed Doktor[1], Mohammad Aarif Siddiqui[1] and Paolo Ceppi[1,2*]

[1]Department of Biochemistry and Molecular Biology, University of Southern Denmark, Campusvej 55, 5230 Odense, Denmark.

[2]Interdisciplinary Centre for Clinical Research, University Hospital Erlangen, FAU-Erlangen-Nuremberg, Erlangen, Germany

[3]Department of Molecular Biology and Genetics, Bilkent University, 06800, Ankara, Turkey.

[#]These authors contributed equally to the work

**Correspondence: pceppi@bmb.sdu.dk (Paolo Ceppi)*

Running title: Pathways and metabolic processes of pyrimidine metabolism in cancer

Abstract

Deregulated nucleotide metabolism, and in particular increased pyrimidine metabolism (PyMet), has been shown to contribute to various pathological features of cancer including chemoresistance and epithelial-to-mesenchymal transition. However, cancer often encompasses complex signaling and metabolic pathway cascades for its progression, and understanding of these molecular regulatory processes in pyrimidine metabolism is quite limited. Therefore, a comprehensive pan-cancer analysis in around 10,000 gene expression profiles of 32 cancer types was employed using a pathway-based approach utilizing gene-sets representing various signaling and metabolic pathways. The analysis identified several top connections with PyMet including TERT, MTOR, DAX1, HOXA1, TP53 and TNC implying an inter-dependency of regulations which in turn was linked to the chemoresistance mechanisms. PyMet-signaling interactions were validated with *in vitro* derived gene-sets from endogenous thymidylate synthase (*TYMS)*-promoter activity reporter, from *TYMS* knockdown and from brequinar treatment, and further at single cell transcriptome level. Strikingly, brequinar treatment profile showed a strong inverse association pattern with doxorubicin chemoresistance in multiple cancer types. The study highlights the PyMet-pathway interactions and its role in chemoresistance, thereby providing an effective tool for improving PyMet targeting strategy in cancer. The analysis as an accessible resource is available at: www.pype.compbio.sdu.dk

Keywords: Pyrimidine metabolism, signaling pathways, metabolic process, brequinar, pan-cancer

Highlights

Pan-cancer analysis showed pyrimidine metabolism connections with signaling pathways

Top pathway interactors of pyrimidine metabolism were TERT, HOXA1, TP53 and TNC

In vitro derived pyrimidine gene-sets recapitulate cancer patients' pathway analysis

Pyrimidine associated pathways confer chemoresistance in multiple cancer types

Pyrimidine metabolic inhibitor brequinar reversed doxorubicin chemoresistance feature

Manuscript Details

Words – 4536

Main Figures – 5

Supplementary Figures – 4

Supplementary Tables – 10

Supplementary Method - 1

References – 44

Introduction

Cancer, a highly heterogenous disease, often characterized with genetic and epigenetic aberrations lead to the accumulation of mutations, deregulated signaling pathways and aberrant metabolic processes in the cell, which in turn facilitates uncontrolled proliferative ability, immune evasion, metastasis and chemoresistance (Hanahan & Weinberg, 2011). Breast, lung and colorectal cancers are the most commonly diagnosed cancers, with lung cancer being the leading cause of cancer-related death (Sung *et al*, 2021). Various curative options have been developed in recent years with survival improvement, although found effective when the disease is diagnosed at early stages (Crosby *et al*, 2022). Improvements in treatment options such as CAR-T cell therapy for hematologic cancers (Dagar *et al*, 2023), immunotherapy for NSCLC and melanoma (André *et al*, 2020; Wang *et al*, 2022), molecular targeted therapy for EGFR mutants with osimertinib in lung cancer (Ramalingam *et al*, 2020), and for HER2-positive breast cancer with tucatinib (Lee, 2020) have shown remarkable success in cancer combating. However, the overall survival rate and response rate remains low for many cancer types. For instance, 5-year overall survival rate of NSCLC is 25% (Caini *et al*, 2022) and for advanced endometrial cancer is 17% (Marth *et al*, 2022). Furthermore, the growing concern about the emergence of drug resistance in cancer patients underscores the challenges associated with the promising chemotherapeutic regimen, leading to disease recurrence and contributing to as much as 90% of cancer-related mortality (Bukowski *et al*, 2020; Ramos *et al*, 2021). All these implying the need for better characterization of cellular and molecular level processes of cancer to exploit therapeutic interventions.

Among the hallmarks of cancer, the foremost feature of cancer cell is to induce uncontrolled proliferation, which in turn is heavily relied on the metabolism of purines and pyrimidines (Mullen & Singh, 2023). Several studies showed that higher expression levels of rate-limiting enzymes of pyrimidine metabolism were observed in more than 80% of cancer types including in lung and liver cancer (Wang *et al*, 2020), breast cancer (Luo *et al*, 2022), gastric cancer (Wu *et al*, 2021) and in acute myeloid leukemia (Wang *et al*, 2021) implicating a strong involvement of pyrimidine metabolism in cancer. Of note, high urea cycle dysregulation (UCD) in cancer contributes to poor prognosis, and showed a significant higher pyrimidine-to-purine ratio in multiple tumors (Lee *et al*, 2018) suggesting the importance of pyrimidine metabolism in tumorigenesis. Besides cellular proliferation, pyrimidine metabolism has also been shown to have prominent roles in several other tumorigenic features such as thymidylate synthase (TS) induced epithelial-to-mesenchymal transition (EMT) mediated metastasis and chemoresistance in breast and lung cancer (Siddiqui *et al*, 2017; Siddiqui *et al*, 2019; Siddiqui *et al*, 2021), and dihydroorotate dehydrogenase (DHODH) involvement in liver metastasis in colorectal cancer (Yamaguchi *et al*, 2019). Indeed, during doxorubicin or cisplatin resistance, an increased *de novo* pyrimidine metabolic flux of dCTP and dTTP pools facilitates DNA repair under genotoxic stress have been observed in triple negative breast cancer (Brown *et al*, 2017). However, tumor development is highly governed by the deregulation in multiple transcriptional programs via signaling pathways and metabolic processes, and oncogenes are tightly connected with the signaling process in mediating the utilization of pyrimidine metabolism both during transcriptional gene activities and at post-translational levels on the metabolic enzymes (Wang *et al*, 2021). Therefore, a comprehensive understanding of the regulatory network behind pyrimidine metabolism is required to provide a better opportunity for

120 therapeutic exploitation of cancer (Sanchez-Vega *et al*, 2018), and to combat drug
121 resistance in cancer.
122
123 Advent of next generation sequencing platforms offered massive molecular insights of
124 cancers, by utilizing the transcriptomic profiles of cancer patients, from unraveling the
125 functional level biological processes behind tumorigenesis to clinical outcome (Bass *et al*,
126 2014; Demircioğlu *et al*, 2019; Frost *et al*, 2020; Thennavan *et al*, 2021; Fäldt Beding *et al*,
127 2022). Therefore, in the present study, an unprecedented intricate role of pyrimidine
128 metabolism in cancer has been addressed by utilizing the transcriptomic profiles of 32
129 cancer types from The Cancer Genome Atlas (TCGA), and explored the signaling pathways
130 and metabolic processes that could be involved in the regulation of pyrimidine metabolism
131 (PyMet).
132
133 **Results**
134 **A comprehensive pan-cancer analysis has identified pyrimidine metabolic-pathway**
135 **connections**
136 Initially, the dependency of pyrimidine metabolism genes in cancer was analyzed by
137 exploring a genome-wide CRISPR/Cas9 knockout screening for fitness genes in 324 cancer
138 cell lines from 30 cancer types (Behan *et al*, 2019). Pyrimidine metabolic gene-set was
139 obtained from KEGG database with the removal of polymerase containing genes to have
140 more metabolism-focused analysis (**Supplementary Table S1**). Pan-cancer fitness analysis
141 of PyMet genes showed that around 20% of the genes were cancer-dependent genes based
142 on the priority scores (**Figure 1A**), and among them the majority were rate-limiting enzymes
143 with thymidylate synthase (*TYMS)* as the top ranked gene (30/2852). This implies a strong

144 role for pyrimidine metabolism in cancer development and progression across cancer types.
145 To comprehensively understand the molecular aspects of pyrimidine metabolic genes role
146 in cancer, identifying signaling pathways and metabolic processes associated with
147 pyrimidine metabolism is essential. Therefore, a pathway-based activity pattern analysis
148 was employed in assessing the signaling pathways or metabolic processes using gene-sets
149 in the tumor mRNA expression profiles of The Cancer Genome Atlas (TCGA). First, a total
150 of 10,071 normalized gene expression profiles of TCGA representing 32 cancer types of 12
151 different cancer origins were collected from cBioportal search engine (**Figure 1B** and
152 **Supplementary Table S2**). Second, multiple gene-sets (n = 585) representing various
153 signaling pathways and metabolic processes were collected from MSigDB (**Supplementary**
154 **Tables S3 and S4**). The activation scores of the gene-sets for PyMet, signaling pathways
155 and metabolic processes were then assessed in each tumor sample using *z*-score based
156 method. Third, the activation scores of the signaling and metabolic pathways were
157 associated with the pyrimidine metabolic process activity scores in each cancer type using
158 Pearson's correlation with clinically accepted correlation range (r < -0.3 and r > 0.3), and
159 further analyzed significantly associated pathways of PyMet across 32 cancer types by
160 meta-correlation (**Supplementary Tables S5 and S6**). From the analysis, we identified top
161 strong positively (meta-r = 0.41 to 0.57; meta-*P*-value < 0.0001) and negatively (meta-r = -
162 0.39 to -0.52; meta-*P*-value < 0.0001) associated pathways of PyMet in more than 20 cancer
163 types (~65% of the cancer types) as threshold (**Figure 1C** and **Supplementary Table S5**).
164 TERT, ESRRA and CAMP pathways were found positively associated with PyMet in around
165 80% of the cancer types, while TNC target gene-set was found negatively associated in 78%
166 of the cancer types. Pathways associations in lung adenocarcinoma (N = 510), as a
167 representative of the cancer types, clearly showed the trend in the positive and negative

168 pathway activity levels with the increase in the PyMet activation score (**Figure 1D**). Few
169 connections with inflammatory signaling were also observed. While around 65% of the
170 cancer types showed negative association of PyMet with interferon beta (meta-r = -0.46),
171 few positive connections were found with IL15 (meta-r = 0.40) and IL2 (meta-r = 0.37) in
172 around 55 to 60% of the cancer types (**Supplementary Table S5**). As expected, across 32
173 cancer types, we also observed other signaling pathways or transcription factor-mediated
174 associations with PyMet such as MYC (meta-r = 0.32 to 0.40), CCND1 & CDK4 (meta-r =
175 0.43), KRAS (meta-r = 0.43), EMT process or cellular transformation signatures (meta-r =
176 0.25 to 0.38) and a negative association with TP53 targets (meta-r = -0.39). We have
177 included, when available, multiple gene-sets for the same pathways derived from different
178 experimental settings or sources such as with MYC and TERT which concordantly showed
179 a similar positive association patterns with PyMet indicating the sensitivity of the approach
180 (**Supplementary Table S5**). The top positively and negatively associated metabolic
181 processes with PyMet were also validated with 2 additional PyMet gene-sets (KEGG
182 pyrimidine and REACTOME pyrimidine) in the largest cancer type cohorts of breast invasive
183 carcinoma (N = 1082), colon adenocarcinoma (N = 592) and uterine corpus endometrial
184 carcinoma (N = 527) revealing the sensitivity in detecting the regulatory connections using
185 pathway-based approach (**Supplementary Figures 1A-C** and **Supplementary Table S7**).
186
187 In parallel, the metabolic processes associated with PyMet were also explored. As
188 anticipated, positive associations were observed between PyMet and nucleotide
189 metabolisms, synthesis of DNA, TCA cycle, OXPHOS and mitotic or cell cycle processes in
190 about 80 to 90% of the cancer types. A pronounced significant negative associations of
191 glutamine deprivation (meta-r = -0.62), leucine deprivation (meta-r = -0.54) and calcium

192 signaling (meta-r = -0.50) with PyMet were observed across cancer types (**Figure 1E**,
193 **Supplementary Figures S1D,E** and **Supplementary Table S6**). Pyrimidine metabolism
194 showed poor prognosis while TNC signaling showed good prognosis in lung
195 adenocarcinoma patient samples (**Figures 1F and 1G**).
196
197 Collectively, a comprehensive analysis of pathway activation pattern in different types of
198 cancers has identified several positively and negatively associated signaling pathways and
199 metabolic processes of pyrimidine metabolism.
200
201 **Pathways associations with PyMet from cancer patients are recapitulated in cancer**
202 **cell lines**
203 Having identified the top signaling pathway regulators of PyMet in patient derived tumor
204 samples, we further went onto validate its findings *in vitro*. Gene set enrichment analysis
205 (GSEA) of few of the top positive (HOXA1, ESRRA, and FLI1-DAX1) and negative (TNC
206 and SOX4) interactors of PyMet showed a clear increase and decrease, respectively, in the
207 pyrimidine metabolism in a cancer cell line expression profiles (N = 917) categorized as high
208 and low based on the pathway activation levels (**Figures 2A,B** and **Supplementary Figures**
209 **S2A-C**) recapitulating the patient derived tumor expression profiles of TCGA. Independently,
210 a previously reported *de novo* pyrimidine synthesis gene, *TYMS* characterized with the non-
211 proliferative role in EMT mediated metastasis (Siddiqui *et al*, 2021), was utilized to validate
212 the findings. *TYMS*-specific gene-set was derived from the FACS sorting of high (TS^{HIGH})
213 and low (TS^{LOW}) cell population of Calu-1 cell line (lung squamous carcinoma) stably
214 expressing mCherry reporter gene under the control of *TYMS* promoter followed by RNA-
215 seq profiling (**Figure 2C and Supplementary Table S8**). The derived gene-set (TS^{LOW} and

216 TS^{HIGH}) was then used as a proxy of pyrimidine metabolism to examine the functional
217 association between the positive and negative pathways of PyMet, and as a result majority
218 of the pathways showed a similar trend of significant associations as observed in the primary
219 tumors of lung squamous expression profiles (**Figure 2D**). In addition, we used another TS
220 gene-set derived by stable shRNA knockdown of *TYMS* gene in A549 cell line followed by
221 RNA-seq profiling (**Figure 2E** and **Supplementary Table S9**). A similar trend of positive
222 and negative association pattern, although with less significance, was observed with TS
223 knockdown gene-set compared to Calu-1 TS-promoter activity (**Figure 2F**).
224
225 Furthermore, to examine the associations pattern at a single cell expression level, a single
226 cell RNA sequencing of parental A549 cell line (untreated) was explored from our previous
227 study (Ramesh *et al*, 2023), and the analysis revealed a consistent results of positive and
228 negative association of the pathways with the pyrimidine metabolism across 5,203 cells
229 (**Figure 2G**). Remarkably, a cluster-based analysis showed that pyrimidine and its
230 associated positive signaling pathways or metabolic processes were strongly expressed in
231 cluster 1 (**Figure 2H** and **Supplementary Figure S2D**). The negative interacting partners
232 of pyrimidine were only reflected at a minimal level of percent negative expression
233 (**Supplementary Figures S2E** and **S2F**). Overall, co-occurrence pattern of signaling
234 pathway processes and PyMet at the single cell level points out the inherent molecular level
235 regulations and dependency of these identified pathways on pyrimidine metabolism.
236
237 **Functional level depletion of pyrimidine metabolism substantiates the signaling**
238 **pathways interactions**

239 To further substantiate and characterize the involvement of the identified signaling pathways
240 in pyrimidine metabolism, A549 cell line was treated with brequinar (BRQ), an inhibitor of
241 DHODH, a rate limiting enzyme in the initial steps of pyrimidine metabolism (**Figure 3A**).
242 Western blot analysis confirmed the inhibition of TS, a downstream end-product catalyzing
243 enzyme of PyMet, to emphasize the depletion of pyrimidine metabolism in the cells (**Figure**
244 **3B**). Differentially expressed genes were then analyzed from the RNA-seq expression
245 profiling of BRQ treated A549 cells with 1 μM for 72 hours which showed maximum depletion
246 of pyrimidine metabolism (**Figure 3C**, **Supplementary Figures S3A** and **Supplementary**
247 **Table S10**). A significant number of PyMet genes, both *de novo* and salvage, were found in
248 the down-regulated gene list of BRQ including *DHODH*, *TYMS*, *TK1*, *RRM1*, *RRM2* and
249 *UPP1* (**Supplementary Figure S3B**) implying the efficient inhibition of pyrimidine
250 metabolism. Additional independent approaches were carried out to validate the top
251 associated pathways of PyMet in the BRQ treated samples. First, by overlap gene
252 enrichment analysis a significant enrichment of mTORC1 and cell proliferative pathways
253 (MYC and E2F) were observed in the BRQ down-regulated genes, while p53 signaling was
254 enriched in the BRQ up-regulated genes (**Supplementary Figures S3C** and **S3D**). Second,
255 comparison of normalized gene expression of the pathway target genes in the RNA-seq
256 profile of BRQ treated samples with the control revealed a significant up-regulation of TNC
257 and TP53-TP73 target genes with the down-regulation of pyrimidine and FLI1-DAX1 genes
258 (**Figure 3D** and **Supplementary Figures S3E-G**). Third, GSEA analysis was performed in
259 the RNA-seq expression profile of LUAD patient samples categorized as BRQ-high and
260 BRQ-low based on the BRQ gene-set pathway activity scores. The results showed a
261 significant enrichment of HOXA1 down-regulated genes (**Figure 3E**) and TNC up-regulated
262 genes (**Supplementary Figure S3H**) in BRQ-high samples, while HOXA1 up-regulated

263 genes (**Figure 3F**) and pyrimidine (**Supplementary Figure S3I**) enrichment in the BRQ-low
264 samples. Finally, a correlation analysis of the pathway activation scores was also performed
265 in the LUAD patient gene expression profile for PyMet and its associated pathways along
266 with the BRQ gene-set. Interestingly, a striking inverse association pattern was observed
267 between BRQ and pyrimidine's associated pathways except for EZH2 (**Figure 3G**). In fact,
268 BRQ gene-set showed a strong positive associations with TNC (r = 0.88) and TP53-TP73 (r
269 = 0.85), and negative associations with HOXA1 (r = -0.87) and FLI1-DAX1 (r = -0.86) (**Figure**
270 **3H**). Further, BRQ treated A549 and SKMES1 cell lines showed an increase in TNC and
271 decrease in DAX1 protein levels (**Figure 3I** and **Supplementary Figures 3J,K**). Similarly,
272 functionally active phosphorylated form of P53 protein level was found increased with BRQ
273 treatment with a decrease in the KRAS (**Figure 3J**). In addition, knockdown of TS in A549
274 cell line markedly decreased the phosphorylated form of MTOR and DAX1 while increased
275 the TNC and P16 protein levels compared to the control (**Figure 3K**) concordant with the
276 transcriptome data (**Figure 2F**). Collectively, *in vitro* pyrimidine metabolic inhibitor treatment
277 with BRQ confirms the pathways associations identified from the patients derived
278 transcriptome analysis.
279

280 **Pyrimidine metabolism and its associated pathways confer chemoresistance in**
281 **multiple cancer types**

282 As pyrimidine metabolism is involved in various clinical manifestations of tumorigenesis from
283 uncontrolled proliferation, EMT and chemoresistance, we investigated whether the identified
284 PyMet associated signaling pathways also have any involvement with chemoresistance.
285 Therefore, we assessed pathway-based activation scores for multiple gene-sets related to
286 various drugs used in the clinic for multiple cancer types such as fluorouracil, cisplatin,

287 gefitinib, gemcitabine and doxorubicin, the activity of which is well known to be limited by
288 chemoresistance. Among the investigated chemoresistance gene-sets, we identified a very
289 strong positive pattern between doxorubicin chemoresistance and PyMet and its associated
290 pathways. Interestingly, this pattern was found to have inverse association with BRQ in
291 pancreatic and lung adenocarcinoma patient samples (**Figures 4A-D**) indicating that BRQ
292 could potentially reverse the effect of doxorubicin chemoresistance. This pattern of positive
293 interaction between doxorubicin chemoresistance and PyMet's associated pathways, and
294 the reversal effect of BRQ was found in multiple cancer types including in breast, bladder
295 and low grade glioma (**Supplementary Figure S4**). Notably, the correlation was significantly
296 strong between doxorubicin resistance and PyMet ($r > 0.5$) or HOXA1 ($r > 0.6$). Conversely,
297 a strong negative correlation was observed between doxorubicin resistance and BRQ ($r = -$
298 0.76 to -0.87) or TNC ($r = -0.86$ to -0.91) (**Figures 4B** and **4D**). Independently, TNC signaling
299 pathway was found enriched in the gene expression profile of neuroblastoma cell line IMR32
300 treated with another DHODH inhibitor, teriflunomide (GSE67338) (**Figure 4E**). Minimal
301 levels of positive associations were also observed with other chemoresistance drugs such
302 as cisplatin and gemcitabine. However, analyzing the gene expression pattern of rate-
303 limiting enzymes of PyMet in cisplatin-resistant A549 cell line (**Figure 4F**) or gemcitabine-
304 resistant Calu-3 cell line (**Figure 4G**) revealed an increased expression with the
305 chemoresistance development.
306
307 Taken together, pathway-based analysis revealed a strong involvement of pyrimidine and
308 its associated pathways in drug resistance, and importantly this involvement could be
309 sensitized or inhibited with DHODH inhibitors.
310

311 **Pyrimidine Pathway Explorer (PYPE) as a web resource to examine pyrimidine**
312 **metabolism regulatory process**

313 Having observed the potential of pathway-based approach in identifying the association
314 patterns between PyMet and signaling pathways or metabolic processes, we developed a
315 web portal as a resource for the scientific community (**Figure 5A**). Pyrimidine Pathway
316 Explorer (PYPE) allows exploration of connections between the signaling pathways or
317 metabolic processes at the gene expression based level: First, signaling pathways or
318 metabolic processes correlations with PyMet in individual cancer types and multiple cancer
319 types can be explored using the PYPE tool. Each separate section for signaling pathways
320 (247 gene-sets) and metabolic processes (335 gene-sets) were included in the entry page.
321 By selecting the cancer type and correlation type, the result output generates a list of
322 correlated signaling or metabolic processes gene-sets with PyMet. Further selecting the
323 gene-set in the obtained list, the activation scores across samples, correlation plot between
324 the signaling (or metabolic process) and PyMet, and finally the overlap of gene list between
325 the gene-sets are obtained. Second, a custom correlation analysis section has been
326 provided wherein the users can input their own gene-sets derived from microarray or RNA-
327 seq from different experimental settings. Both options of inputting single or paired direction
328 gene-sets can be imputed by the web tool. The results include the correlation between
329 PyMet gene-set and user-defined gene-set for each individual cancer type. Further, when
330 selected multiple cancer types, a Forest plot of meta-correlation values across selected
331 cancer types can be obtained. In another tab, an overlap analysis report will also be
332 generated between the user-defined gene-sets and PyMet gene-set. We cross-validated our
333 gene-sets derived from TS^{LOW}/TS^{HIGH} from Calu-1 and TS-knockdown gene-set from A549
334 cells in PYPE across cancer types, and identified that majority of the cancer types showed

335 PyMet associations in a significant manner for TS specific gene-sets (**Figures 5B,C**). The
336 developed web server provides a flexible analysis of gene expression based analysis of
337 pyrimidine metabolism in the aspects of signaling pathways and metabolic processes
338 (**Figure 5D**). The findings as an accessible resource is available at:
339 www.pype.compbio.sdu.dk
340

341 **Discussion**

342 Deregulated pyrimidine metabolism contributes to sustained cell proliferation, genome
343 instability, deregulation of cellular bioenergetics, and further conferring advanced
344 tumorigenic features including EMT-mediated metastasis with worse prognosis (Wang *et al*,
345 2020). In the current pan-cancer study, by utilizing several thousands of gene expression
346 profiles of 32 cancer types, we explored the intricate regulatory network of signaling and
347 metabolic pathways with pyrimidine metabolism using pathway-based approach. Many of
348 the identified associations in this study were also reported previously like with TERT
349 (Mannherz & Agarwal, 2023), KRAS (Koundinya *et al*, 2018) and CCND1 (Qian *et al*, 2020).
350 For instance, thymidine nucleotide metabolic genes (*TYMS*, *DTYMK*, *TK1* and *DCTPP1*)
351 were found to strongly regulate telomere length maintenance identified from a genome-wide
352 CRISPR-Cas9 functional screening (Mannherz & Agarwal, 2023). And PyMet negative
353 partner p53 signaling pathway identified from the current study was also observed previously
354 wherein p53 pathway was activated upon the depletion of pyrimidines relied on DHODH
355 (Khutornenko *et al*, 2010). Similarly, at the metabolic level, dependency of oxidative
356 phosphorylation on pyrimidine metabolism was also in line with the earlier observation
357 wherein regulation of pyrimidine metabolism driven by DHODH is essential in functional
358 oxidative phosphorylation for tumorigenesis (Bajzikova *et al*, 2019). This confirms the

359 sensitivity of the pathway-based approach and its reliability in exploring novel molecular
360 regulatory connections. The involvement of proliferative pathways and EMT associations
361 with pyrimidine metabolism from the pathway analysis indeed support the model of
362 differential contributions of pyrimidine metabolism in cancer (Siddiqui *et al*, 2019).
363 Interestingly, the analysis also identified few novel signaling pathways such as HOXA1 and
364 TNC signaling pathways in the positive and negative regulation of pyrimidine metabolism,
365 respectively, in more than 24 cancer types (>75%) which would be of relevance for future
366 explorations.
367
368 Next, a strong recapitulation of the connections between pyrimidine and signaling pathways
369 were also validated using multiple different genomic approaches. First, with CCLE
370 containing 917 cell lines derived from different cancer subtypes. Second, by functionally
371 modulating a principal component gene, *TYMS*, of pyrimidine metabolism both at the gene
372 knockdown level and by capturing endogenous pyrimidine metabolic level from *TYMS*-
373 driven promoter activity. The observation of low significance with *TYMS* knockdown gene-
374 set compared to *TYMS*-driven promoter gene-set in pathways associations could be due to
375 the capturing of the upstream and downstream pathways from undisrupted endogenous
376 level of pyrimidine metabolism with *TYMS*-promoter activity while *TYMS* knockdown could
377 capture only the downstream associated molecular processes. Third, at the single cell RNA
378 sequencing of a parental lung cancer cell line (without any treatment) implying that these
379 regulatory processes are inherent at the cellular level. Previously, chemical synthetic lethal
380 screening has identified DHODH as a target of mutant KRAS, and inhibition of DHODH with
381 brequinar selectively inhibited *in vitro* and *in vivo* KRAS driven cancerous growth including
382 lung (Koundinya *et al*, 2018). Strikingly, this is in line with our study on the significant inverse

383 association between the brequinar gene-set and KRAS mutant activation levels in lung
384 cancer (**Supplementary Figure S3L**). In addition, the derived brequinar gene-set has also
385 shown a precise inverse pattern to the pyrimidine-associated pathways such as HOXA1,
386 MTOR, CCND1-CDK4 and FLI1-DAX1 in the patient derived gene expression profiles
387 indicating a strong regulatory phenomenon by pyrimidine metabolism at the cellular level
388 and high relevance of these targets in synthetic lethality in cancers dependent on pyrimidine
389 metabolism. In fact, a recent screening of inhibitors for FLI1-DAX1 has identified K-234, a
390 DHODH inhibitor, for Ewing's sarcomas (Watanabe *et al*, 2023). Negative effect of TP53
391 with pyrimidine was also observed before when DHODH inhibitor treatment increases TP53
392 levels (Ladds et al., 2018) and substantiated in the current study with an increased
393 phosphorylated-p53 with BRQ treatment. TNC, an extracellular matrix molecule, was found
394 correlated with tumor progression with poor prognosis in multiple cancer types (Liot *et al*,
395 2020). However, our pathway-based analysis showed a negative association pattern with
396 pyrimidine metabolism across cancer types, and notably the regulation of TNC signaling by
397 DHODH inhibitors would be worth investigating in the future. All these convincingly highlight
398 the importance of the identified signaling pathways and pyrimidine metabolism in targeting
399 several types of cancer.
400
401 Cancer drug resistance is an important feature in the recurrence of cancer in patients
402 contributing to poor survival (Ramos *et al*, 2021), and our gene expression analysis of
403 pyrimidine rate limiting enzymes showed a strong pattern of positive regulation of
404 chemoresistance. Strong evidences have shown the importance of DHODH inhibition in
405 sensitizing the cancer cells to overcome the chemoresistance in several cancer types
406 (Madak *et al*, 2019; Zhang *et al*, 2022). Similarly, doxorubicin treatment has been shown to

407 stimulate the increase in the *de novo* pyrimidine synthesis, and pharmacological inhibition
408 of pyrimidine synthesis with leflunomide in combination with doxorubicin has sensitized the
409 TNBC cells (Brown *et al*, 2017). Furthermore, *in vivo* combinatorial treatment of melanoma
410 xenograft with BRQ and doxorubicin had a substantial tumor growth reduction and improved
411 the efficacy of doxorubicin potency (Dorasamy *et al*, 2019). In accordance with these
412 studies, the current study for the first time uncovered the pan-cancer role of signaling
413 pathways and metabolic processes strongly associated with pyrimidine metabolism. And
414 most importantly, it shows that DHODH inhibitor, brequinar, can overcome chemotherapy
415 resistance especially by doxorubicin and cisplatin by targeting multiple signaling pathways
416 dependent on pyrimidine metabolism in several cancer types. Thus, further exploration of
417 the identified signaling regulatory network or metabolic processes of pyrimidine metabolism
418 would help uncover the development of combinatorial therapeutic treatment options for drug
419 resistance cancer types specifically for doxorubicin.
420
421 The pathway-based approach in the study includes advantages and few limitations in the
422 utilization of the gene-sets derived from different sources. The current study included
423 multiple numbers of gene-sets for the same pathway or metabolic processes derived from
424 different studies to have concordant results for the pathway associations. For example, all
425 5 gene-sets of TERT signaling from different studies using different cell line origins showed
426 a consistent positive association with pyrimidine (meta-r = 0.33 to 0.69). Similarly, 5 out of
427 7 hypoxia different gene-sets obtained by HIF1A overexpression or hypoxia mimic
428 treatments showed a consistent negative association with pyrimidine metabolism (meta-r =
429 -0.47 to -0.62) indicating the increased confidence level of the association patterns. On the
430 other hand, we also observed few pathway gene-sets performed in a context-specific

431 manner. For instance, majority of the KRAS mutant gene-sets derived from different tissue
432 types (lung, breast, prostate) showed a similar positive trend in association with pyrimidine
433 metabolism except for kidney, and KRAS gene-set from lung showed strong positive
434 associations with pyrimidine metabolism in around 20 cancer types (62%) compared to other
435 tissue types derived gene-sets. In another instance, pyrimidine metabolism showed a
436 negative association with YBX1 gene-set from ovarian cancer cell line in 75% cancer types
437 and this outperformed breast cancer cell line derived YBX1 gene-set showing positive
438 association in only 38% cancer types. Nevertheless, when tight meta-correlation thresholds
439 were applied, the later was excluded to reduce false positives. The differential effect in
440 association pattern could have been due to the tissue-specific nature and genetic makeup
441 of the cell line used to derive the gene-sets. With stringent parameters set in the pathway-
442 based analysis and by experimentally validating the pathway associations such context-
443 specific variabilities could be eliminated. Further, in future, the sensitivity of the pathway-
444 based approach could be strengthened by expanding the number of gene-sets for signaling
445 and metabolic pathways in pan-cancer manner to derive a conserved or hallmark gene
446 signatures. A conserved pathway gene signature derived from a pan-cancer perspective
447 could be useful to capture a refined and defined biological processes of the cell which in
448 turn can be used to analyze pathways independent of context-specific nature of the studies.
449
450 The current study's results projected as a web tool resource for the scientific community
451 would be helpful in exploring the association between the pyrimidine metabolism and
452 signaling pathways or metabolic processes across cancer types. The major advantage of
453 pathway-based analysis over the conventional over-representation analysis is that the
454 earlier performs at the gene expression levels in the patient samples which provides more

455 reliable output than the later based on gene content overlap. Besides the in-built features in
456 the PYPE tool, the web resource also allows to analyze the associations between the user
457 defined gene list (for instance experimentally derived) and pyrimidine metabolic pathway
458 across several types of cancers providing a platform to explore the oncogenic processes
459 mediated by pyrimidine metabolism and its associated pathways in multiple cancers.
460 Furthermore, the user defined gene-set analysis could also pave a way in identifying a
461 potential impact of chemoresistance and therapeutic targeting of cancer.
462

463 **Conclusion**

464 A comprehensive pan-cancer analysis of pyrimidine metabolism in the context of signaling
465 pathways and metabolic processes showed molecular regulatory connections with clinical
466 features including chemoresistance for oncogenic pyrimidine metabolism. Further, the study
467 highlights the combinatorial therapeutic approach of using DHODH inhibitors to enhance the
468 efficacy of routinely used chemotherapeutic drugs in clinic.
469

470 **Methods**

471 **Cell culture**

472 A549 and SKMES1 cell lines (ATCC) were cultured in DMEM high glucose medium (Gibco)
473 and RPMI-1640 (Gibco), respectively, supplemented with 2 mM of L-glutamine (Gibco), 100
474 U/ml of Penicillin-Streptomycin (Gibco) and 10% Fetal bovine serum (Gibco). Cell lines were
475 maintained at 37° C with 5% CO_2 level in a humidified incubator. Cell lines were
476 authenticated by STR profiling and routinely tested for mycoplasma contamination.
477

478 **Western blot**

479 Around 1 x 10^5 cells were seeded in a 6-well plate for the drug treatment with Brequinar
480 (Tocris, 6196) in a dose-dependent manner for 72 h. After 72 h treatment, cells were
481 harvested for protein using Pierce RIPA lysis buffer (Thermo Scientific) containing 1X Halt
482 Protease & Phosphatase inhibitor cocktail (Thermo Scientific) and estimated the protein
483 concentrations using Pierce BCA Protein Assay Kit as per the manufacturer's protocol
484 (ThermoFisher Scientific). Around 10 µg of proteins were allowed to resolve in 8% SDS-
485 PAGE separating gel, and the proteins were then transferred from the separating gel to a
486 PVDF membrane (Thermo Scientific). Membranes with the transferred proteins were
487 blocked with the blocking buffer (5% non-fat dried milk powder or 3% bovine serum albumin
488 in 1X TBS-T) for 1 hour at room temperature. After blocking, the membranes were then
489 incubated overnight with the primary antibody at 4° C. Primary antibodies used in the study
490 with dilutions were: TS (1:2500, rabbit, abcam, ab108995), TNC (1:1000, rabbit, abcam,
491 ab108930), DAX1 (1:1000, rabbit, abcam, ab196649), KRAS (1:1000, rabbit, abcam,
492 ab180772), p-mTOR (1:1000, rabbit, Cell Signaling, 2971S), p-P53 (1:1000, rabbit, Cell
493 Signaling, 9284S), P16 (1:1000, mouse, abcam, ab54210) and β-Actin HRP conjugated
494 (1:10000, Cell Signaling, 12262). Membranes were washed thrice with 1X TBS-T and
495 incubated with the secondary antibody. Secondary antibodies used were: Goat Anti-rabbit
496 IgG-HRP (1:10000, Southern Biotech, 4030-05) and Goat Anti-mouse IgG2b-HRP (1:10000,
497 Southern Biotech, 1091-05). Pierce ECL western blotting solution (Thermo Scientific) was
498 used to detect the protein bands with the development of X-ray films (Thermo Scientific).
499

500 **RNA-sequencing**

501 A549 cell line treated with brequinar was harvested for RNA using 700 µl of QIAzol reagent
502 (Qiagen), and the total RNA was isolated and eluted in 40 µl of nuclease free water (VWR)

503 as per the manufacturer's protocol using miRNeasy kit (Qiagen). 500 ng of total RNA was
504 utilized to construct the sequencing libraries using NEBNext Ultra RNA Library Prep Kit for
505 Illumina as per the manufacturer's protocol (NEB) and paired-end sequencing was
506 performed with NovaSeq 6000 platform (Illumina).
507
508 RNA-seq analysis was performed with the obtained Fastq files from the sequencing
509 platform. Briefly, quality control (QC) analysis was carried out using FastQC program
510 followed by the alignment of the reads to the reference genome GRCh38 release 105 along
511 with the respective human gene annotation file using STAR aligner v2.7.9a. The aligned
512 reads were then counted using the featureCounts function in Rsubread v2.10.5 package in
513 R 4.2.1. Differential gene expression analysis was performed using the raw count reads with
514 DESeq2 v1.36.0 package in R with an adjusted p-value<0.0001 and fold change of 2.
515
516 **Single cell RNA-sequencing**
517 Single cell RNA sequencing for parental A549 cell line was performed using 10X Genomics
518 guidelines at the Institute of Human Genetics, Friedrich-Alexander-University of Erlangen-
519 Nürnberg, Erlangen, Germany. Approximately 6000 cells were used and obtained 25,000
520 reads per cell. In brief, cellranger-4.0.0 pipeline was used to obtain the
521 filtered_feature_bc_matrix data and analyzed further with Seurat v4.2.1 package in R. Pre-
522 processing of the file was performed after quality control metric analysis and filtered the data
523 by eliminating cells with less than 500 genes, UMIs with <2500 & >45000 total number of
524 molecules, >10% mitochondrial genes and with > 5% largest genes. Log_{10} genes per UMI
525 was set at > 0.85 for filtering. Normalization of the counts was done with the library size
526 normalization and selected 2000 variable genes to perform principal component analysis

527 (PCA). For the downstream analysis, cells were regressed out for the variations including
528 mitochondrial genes, cell cycle genes, and genes & UMI counts per cell. With the first 25
529 principal components, cell clusters were determined using Lovain algorithm with a resolution
530 of 0.4, and tSNE dimensionality reduction method was employed to visualize the cell
531 clusters. AddModuleScore function in Seurat was then applied to assess the percent
532 activation pattern of pyrimidine and its associated signaling or metabolic processes gene-
533 sets for the up-regulated gene-sets in the identified cell clusters.
534

535 **Gene enrichment analysis**

536 Gene set enrichment analysis (GSEA) was performed for the patient samples and cancer
537 cell line gene expression profile by categorizing the samples as low and high based on the
538 median of the z-score activation levels of the gene-sets. Signal2Noise metric was used to
539 rank the genes between groups comparison. Significance for the enrichment was set at a
540 nominal p-value < 0.05 and FDR < 0.25. Representational overlap analysis of BRQ-
541 regulated genes identified from RNA-seq analysis was performed with Enrichr web tool
542 (Kuleshov *et al*, 2016) containing in-built gene-set libraries for various biological functions.
543

544 **Survival analysis**

545 Samples from TCGA gene expression profiles obtained from cbioportal platform were
546 categorized as low and high based on the median of the signaling pathways gene-set activity
547 score calculated with the difference of up-regulated and down-regulated activation scores in
548 the patient samples. Survival curves were generated based on Kaplan-Meier estimate
549 analysis with log-rank test used to estimate the significant difference between the two
550 categorized groups and hazard ratio was estimated using Cox proportional in R software.

551

552 **Gene-sets source**

553 Signaling pathways and metabolic process associated gene-sets were collected from
554 MSigDb v6.2. In total, 247 signaling associated gene-sets and 335 metabolic process
555 associated gene-sets were collected (135 of KEGG and 200 of REACTOME gene-sets).
556 Signaling pathway gene-sets represent oncogenic, tumor suppressor, epigenetic, stem
557 cells, cell cycle and transcription factor mediated pathways. Metabolic process associated
558 gene-sets collectively represent diverse metabolic processes of the cell such as fatty acids,
559 steroids, vitamins, lipids, carbohydrates, organic, inorganic, catabolic and anabolic
560 reactions, amino acids, hormones, nucleotide, enzymatic activities including coenzymes or
561 co-factors, alcohol, amine, drug, acyl chain related metabolisms, biopolymer and
562 macromolecular metabolism. Pyrimidine metabolism gene-set was collected from KEGG
563 database and the polymerase containing genes were removed from the list to have more
564 metabolism-centered analysis.

565

566 **Pathway-based activation analysis**

567 Signaling pathway or metabolic process activity score was calculated as described
568 previously (Ramesh & Ganesan, 2016). First, fold difference ($\log_2$) for each gene in each
569 tumor sample was calculated relative to the median expression value across tumor samples
570 of each cancer subtype as reference. Second, mean and standard deviation for each tumor's
571 whole gene expression profile was calculated. Third, mean of the fold expression value for
572 each signaling pathway or metabolic processes genes in the gene-sets was calculated for
573 each tumor sample. Next, pathway or metabolic process activity score (z-score) was
574 estimated by subtracting the mean fold expression value of the whole gene expression from

575 the mean fold expression value of the gene-set followed by dividing by standard deviation
576 of the whole gene expression profile of the tumor sample. Finally, a normalized activation
577 score of the gene-set was obtained by multiplying the obtained above score with the square
578 root of the number of genes in the gene-set. In case of pathways containing up- and down-
579 regulated gene-sets, the final normalized activation score was further obtained by
580 subtracting down-score from the up-score. Normalized activation scores were then used to
581 assess the association between PyMet and the signaling or metabolic process gene-sets by
582 Pearson's correlation method with significance calculation. Percent positive and negative
583 rate of correlations across cancer types were calculated with adjusted p-value < 0.05 and r
584 > 0.3 or r < -0.3. Then, the number of cancer types with PyMet associated gene-sets
585 (signaling or metabolic) was counted as positive or negative after threshold filtering. To
586 strengthen the observed association pattern, a meta-correlation analysis was performed
587 using metacor.DSL function in R for the tumor types satisfying the initial Pearson's
588 correlation threshold. The number of samples in each dataset was included for the meta-
589 correlation analysis and significantly associated gene-sets were identified with meta-r > 0.3
590 and meta-r < -0.3 as positively and negatively associated, respectively, with meta-p-value <
591 0.05. Heatmap representation of the activation scores or correlation values was carried out
592 using R v4.2.1 or GraphPad Prism9 software. A detailed programming script for calculating
593 the pathway activation scores, correlation analysis and meta-analysis is provided in the
594 **Supplementary Method** section. PYPE web application was developed using Shiny
595 package in the R environment.
596
597 **Statistical analysis**

598 All statistical analysis was performed using GraphPad Prism9 software or using R v4.2.1
599 software.
600
601 **Data Availability**
602 The RNA-seq profile of brequinar treatment produced in this study was deposited in Gene
603 Expression Omnibus database with the accession number: GSE248686
604 (https://www.ncbi.nlm.nih.gov/geo/query/acc.cgi?acc=GSE248686)
605
606 **Acknowledgements**
607 This work was supported by the Interdisciplinary Center for Clinical Research of the
608 University of Erlangen-Nuremberg, the German Research Foundation (DFG, CE 281/6-1),
609 the Novo Nordisk Foundation (Hallas-Møller Ascending Investigator Grant 0066909), and
610 by the Danish Cancer Society (A18859). Research work of MAS is supported by Lundbeck
611 Foundation, Denmark (R380-2021-1264). Sequencing was performed at the Center for
612 Functional Genomics and Tissue Plasticity, Functional Genomics & Metabolism Research
613 Unit, University of Southern Denmark. The authors thank Tenna P. Mortensen, Maibrith
614 Wishoff and Ronni Nielsen for sequencing assistance.
615
616 **Disclosure statement and competing interests**
617 The authors declare that they have no conflict of interest.
618
619 **Author's contribution**
620 Conceived the concept: VR and PC; Designed the experiments: VR and PC; Performed the
621 experiments: VR, LP and MAS. Performed computational and statistical analysis: VR and

622 MD; Designed web server: VR, MD and TKD; Wrote the manuscript: VR and PC. All the
623 authors read and approved the final manuscript.
624
625 **Reference**

626 André T, Shiu KK, Kim TW, Jensen BV, Jensen LH, Punt C, Smith D, Garcia-Carbonero R,
627 Benavides M, Gibbs P *et al* (2020) Pembrolizumab in Microsatellite-Instability-High
628 Advanced Colorectal Cancer. *The New England journal of medicine* 383: 2207-2218
629 Bajzikova M, Kovarova J, Coelho AR, Boukalova S, Oh S, Rohlenova K, Svec D, Hubackova
630 S, Endaya B, Judasova K *et al* (2019) Reactivation of Dihydroorotate Dehydrogenase-
631 Driven Pyrimidine Biosynthesis Restores Tumor Growth of Respiration-Deficient Cancer
632 Cells. *Cell metabolism* 29: 399-416.e310
633 Bass AJ, Thorsson V, Shmulevich I, Reynolds SM, Miller M, Bernard B, Hinoue T, Laird PW,
634 Curtis C, Shen H *et al* (2014) Comprehensive molecular characterization of gastric
635 adenocarcinoma. *Nature* 513: 202-209
636 Behan FM, Iorio F, Picco G, Gonçalves E, Beaver CM, Migliardi G, Santos R, Rao Y, Sassi
637 F, Pinnelli M *et al* (2019) Prioritization of cancer therapeutic targets using CRISPR-Cas9
638 screens. *Nature* 568: 511-516
639 Brown KK, Spinelli JB, Asara JM, Toker A (2017) Adaptive Reprogramming of De Novo
640 Pyrimidine Synthesis Is a Metabolic Vulnerability in Triple-Negative Breast Cancer. *Cancer*
641 *discovery* 7: 391-399
642 Bukowski K, Kciuk M, Kontek R (2020) Mechanisms of Multidrug Resistance in Cancer
643 Chemotherapy. *International journal of molecular sciences* 21
644 Caini S, Del Riccio M, Vettori V, Scotti V, Martinoli C, Raimondi S, Cammarata G, Palli D,
645 Banini M, Masala G *et al* (2022) Quitting Smoking At or Around Diagnosis Improves the

646 Overall Survival of Lung Cancer Patients: A Systematic Review and Meta-Analysis. *Journal*
647 *of thoracic oncology : official publication of the International Association for the Study of*
648 *Lung Cancer* 17: 623-636
649 Crosby D, Bhatia S, Brindle KM, Coussens LM, Dive C, Emberton M, Esener S, Fitzgerald
650 RC, Gambhir SS, Kuhn P *et al* (2022) Early detection of cancer. *Science (New York, NY)*
651 375: eaay9040
652 Dagar G, Gupta A, Masoodi T, Nisar S, Merhi M, Hashem S, Chauhan R, Dagar M, Mirza
653 S, Bagga P *et al* (2023) Harnessing the potential of CAR-T cell therapy: progress,
654 challenges, and future directions in hematological and solid tumor treatments. *Journal of*
655 *translational medicine* 21: 449
656 Demircioğlu D, Cukuroglu E, Kindermans M, Nandi T, Calabrese C, Fonseca NA, Kahles A,
657 Lehmann KV, Stegle O, Brazma A *et al* (2019) A Pan-cancer Transcriptome Analysis
658 Reveals Pervasive Regulation through Alternative Promoters. *Cell* 178: 1465-1477.e1417
659 Dorasamy MS, Ab A, Nellore K, Wong PF (2019) Synergistic inhibition of melanoma
660 xenografts by Brequinar sodium and Doxorubicin. *Biomedicine & pharmacotherapy =*
661 *Biomedecine & pharmacotherapie* 110: 29-36
662 Fäldt Beding A, Larsson P, Helou K, Einbeigi Z, Parris TZ (2022) Pan-cancer analysis
663 identifies BIRC5 as a prognostic biomarker. *BMC cancer* 22: 322
664 Frost FG, Cherukuri PF, Milanovich S, Boerkoel CF (2020) Pan-cancer RNA-seq data
665 stratifies tumours by some hallmarks of cancer. *Journal of cellular and molecular medicine*
666 24: 418-430
667 Hanahan D, Weinberg RA (2011) Hallmarks of cancer: the next generation. *Cell* 144: 646-
668 674

669 Khutornenko AA, Roudko VV, Chernyak BV, Vartapetian AB, Chumakov PM, Evstafieva AG
670 (2010) Pyrimidine biosynthesis links mitochondrial respiration to the p53 pathway.
671 *Proceedings of the National Academy of Sciences of the United States of America* 107:
672 12828-12833
673 Koundinya M, Sudhalter J, Courjaud A, Lionne B, Touyer G, Bonnet L, Menguy I, Schreiber
674 I, Perrault C, Vougier S *et al* (2018) Dependence on the Pyrimidine Biosynthetic Enzyme
675 DHODH Is a Synthetic Lethal Vulnerability in Mutant KRAS-Driven Cancers. *Cell chemical*
676 *biology* 25: 705-717.e711
677 Kuleshov MV, Jones MR, Rouillard AD, Fernandez NF, Duan Q, Wang Z, Koplev S, Jenkins
678 SL, Jagodnik KM, Lachmann A *et al* (2016) Enrichr: a comprehensive gene set enrichment
679 analysis web server 2016 update. *Nucleic acids research* 44: W90-97
680 Lee A (2020) Tucatinib: First Approval. *Drugs* 80: 1033-1038
681 Lee JS, Adler L, Karathia H, Carmel N, Rabinovich S, Auslander N, Keshet R, Stettner N,
682 Silberman A, Agemy L *et al* (2018) Urea Cycle Dysregulation Generates Clinically Relevant
683 Genomic and Biochemical Signatures. *Cell* 174: 1559-1570.e1522
684 Liot S, Aubert A, Hervieu V, Kholti NE, Schalkwijk J, Verrier B, Valcourt U, Lambert E (2020)
685 Loss of Tenascin-X expression during tumor progression: A new pan-cancer marker. *Matrix*
686 *biology plus* 6-7: 100021
687 Luo Y, Tian W, Lu X, Zhang C, Xie J, Deng X, Xie Y, Yang S, Du W, He R *et al* (2022)
688 Prognosis stratification in breast cancer and characterization of immunosuppressive
689 microenvironment through a pyrimidine metabolism-related signature. *Frontiers in*
690 *immunology* 13: 1056680

691 Madak JT, Bankhead A, 3rd, Cuthbertson CR, Showalter HD, Neamati N (2019) Revisiting
692 the role of dihydroorotate dehydrogenase as a therapeutic target for cancer. *Pharmacology*
693 *& therapeutics* 195: 111-131
694 Mannherz W, Agarwal S (2023) Thymidine nucleotide metabolism controls human telomere
695 length. *Nature genetics* 55: 568-580
696 Marth C, Tarnawski R, Tyulyandina A, Pignata S, Gilbert L, Kaen D, Rubio MJ, Frentzas S,
697 Beiner M, Magallanes-Maciel M *et al* (2022) Phase 3, randomized, open-label study of
698 pembrolizumab plus lenvatinib versus chemotherapy for first-line treatment of advanced or
699 recurrent endometrial cancer: ENGOT-en9/LEAP-001. *International journal of gynecological*
700 *cancer : official journal of the International Gynecological Cancer Society* 32: 93-100
701 Mullen NJ, Singh PK (2023) Nucleotide metabolism: a pan-cancer metabolic dependency.
702 *Nature reviews Cancer* 23: 275-294
703 Qian Y, Liang X, Kong P, Cheng Y, Cui H, Yan T, Wang J, Zhang L, Liu Y, Guo S *et al*
704 (2020) Elevated DHODH expression promotes cell proliferation via stabilizing β-catenin in
705 esophageal squamous cell carcinoma. *Cell death & disease* 11: 862
706 Ramalingam SS, Vansteenkiste J, Planchard D, Cho BC, Gray JE, Ohe Y, Zhou C,
707 Reungwetwattana T, Cheng Y, Chewaskulyong B *et al* (2020) Overall Survival with
708 Osimertinib in Untreated, EGFR-Mutated Advanced NSCLC. *The New England journal of*
709 *medicine* 382: 41-50
710 Ramesh V, Ganesan K (2016) Integrative functional genomic analysis unveils the differing
711 dysregulated metabolic processes across hepatocellular carcinoma stages. *Gene* 588: 19-
712 29

713 Ramesh V, Gollavilli PN, Pinna L, Siddiqui MA, Turtos AM, Napoli F, Antonelli Y, Leal-Egaña
714 A, Havelund JF, Jakobsen ST *et al* (2023) Propionate reinforces epithelial identity and
715 reduces aggressiveness of lung carcinoma. *EMBO molecular medicine*: e17836
716 Ramos A, Sadeghi S, Tabatabaeian H (2021) Battling Chemoresistance in Cancer: Root
717 Causes and Strategies to Uproot Them. *International journal of molecular sciences* 22
718 Sanchez-Vega F, Mina M, Armenia J, Chatila WK, Luna A, La KC, Dimitriadoy S, Liu DL,
719 Kantheti HS, Saghafinia S *et al* (2018) Oncogenic Signaling Pathways in The Cancer
720 Genome Atlas. *Cell* 173: 321-337.e310
721 Siddiqui A, Gollavilli PN, Schwab A, Vazakidou ME, Ersan PG, Ramakrishnan M, Pluim D,
722 Coggins S, Saatci O, Annaratone L *et al* (2019) Thymidylate synthase maintains the de-
723 differentiated state of triple negative breast cancers. *Cell death and differentiation* 26: 2223-
724 2236
725 Siddiqui A, Vazakidou ME, Schwab A, Napoli F, Fernandez-Molina C, Rapa I, Stemmler MP,
726 Volante M, Brabletz T, Ceppi P (2017) Thymidylate synthase is functionally associated with
727 ZEB1 and contributes to the epithelial-to-mesenchymal transition of cancer cells. *The*
728 *Journal of pathology* 242: 221-233
729 Siddiqui MA, Gollavilli PN, Ramesh V, Parma B, Schwab A, Vazakidou ME, Natesan R,
730 Saatci O, Rapa I, Bironzo P *et al* (2021) Thymidylate synthase drives the phenotypes of
731 epithelial-to-mesenchymal transition in non-small cell lung cancer. *British journal of cancer*
732 124: 281-289
733 Sung H, Ferlay J, Siegel RL, Laversanne M, Soerjomataram I, Jemal A, Bray F (2021) Global
734 Cancer Statistics 2020: GLOBOCAN Estimates of Incidence and Mortality Worldwide for 36
735 Cancers in 185 Countries. *CA: a cancer journal for clinicians* 71: 209-249

736 Thennavan A, Beca F, Xia Y, Recio SG, Allison K, Collins LC, Tse GM, Chen YY, Schnitt
737 SJ, Hoadley KA *et al* (2021) Molecular analysis of TCGA breast cancer histologic types. *Cell*
738 *genomics* 1
739 Wang DR, Wu XL, Sun YL (2022) Therapeutic targets and biomarkers of tumor
740 immunotherapy: response versus non-response. *Signal transduction and targeted therapy*
741 7: 331
742 Wang H, Wang X, Xu L, Zhang J, Cao H (2020) High expression levels of pyrimidine
743 metabolic rate-limiting enzymes are adverse prognostic factors in lung adenocarcinoma: a
744 study based on The Cancer Genome Atlas and Gene Expression Omnibus datasets.
745 *Purinergic signalling* 16: 347-366
746 Wang W, Cui J, Ma H, Lu W, Huang J (2021) Targeting Pyrimidine Metabolism in the Era of
747 Precision Cancer Medicine. *Frontiers in oncology* 11: 684961
748 Watanabe M, Kosaka H, Sugawara M, Maemoto M, Ono Y, Uemori T, Shizu R, Yoshinari K
749 (2023) Screening for DAX1/EWS-FLI1 functional inhibitors identified dihydroorotate
750 dehydrogenase as a therapeutic target for Ewing's sarcoma. *Cancer medicine* 12: 9802-
751 9814
752 Wu Z, Tan J, Zhuang Y, Zhong M, Xiong Y, Ma J, Yang Y, Gao Z, Zhao J, Ye Z *et al* (2021)
753 Identification of crucial genes of pyrimidine metabolism as biomarkers for gastric cancer
754 prognosis. *Cancer cell international* 21: 668
755 Yamaguchi N, Weinberg EM, Nguyen A, Liberti MV, Goodarzi H, Janjigian YY, Paty PB,
756 Saltz LB, Kingham TP, Loo JM *et al* (2019) PCK1 and DHODH drive colorectal cancer liver
757 metastatic colonization and hypoxic growth by promoting nucleotide synthesis. *eLife* 8

758 Zhang L, Zhang J, Wang J, Ren C, Tang P, Ouyang L, Wang Y (2022) Recent advances of
759 human dihydroorotate dehydrogenase inhibitors for cancer therapy: Current development
760 and future perspectives. *European journal of medicinal chemistry* 232: 114176

761

762 **Figure Legends**

763 **Figure 1. Pathway-based activation analysis of pan-cancer transcriptome profiles has**
764 **identified novel signaling pathways and metabolic processes of pyrimidine**
765 **metabolism.**

766 A. Ranked plot depicting the priority scores of the pan-cancer fitness genes essential for
767 cancer growth and survival. Highlighted dots represent the pyrimidine metabolic genes
768 essential for cancer with the rank indicated in the brackets.

769 B. Pie-Donut representation of 32 cancer types from 12 different tissue origins with the
770 number of samples used in the study.

771 C. Heatmap visualization of correlation values between top positively and negatively
772 associated signaling pathways with PyMet across 32 cancer types.

773 D. Representative heatmap visualization of the activation pattern of top positively and
774 negatively associated pathways of PyMet in the lung adenocarcinoma patient samples (N =
775 510) with the increasing trend of PyMet activation levels as a bar chart above heatmap.

776 E. Correlation plot depicting the negative association between the activation scores of
777 glutamine deprivation and PyMet in stomach adenocarcinoma gene expression profile (N =
778 412).

779 F, G. Overall survival analysis in the TCGA lung adenocarcinoma patient samples
780 categorized as low- and high-levels of pyrimidine metabolic process (F) or TNC signaling
781 (G) based on the median of the activation scores of the gene-sets. HR – Hazard ratio

782 indicated for high-activation scores containing group was calculated using Cox proportional
783 hazards model and *P*-value was calculated using log-rank method.
784
785 **Figure 2. Pathway-based activation analysis in cancer cell lines recapitulate signaling**
786 **pathway associations with pyrimidine metabolic process.**
787 A. Gene-set enrichment analysis of KEGG pyrimidine metabolism gene-set in the gene
788 expression profile of cancer cell line encyclopedia (CCLE) panel (N = 917) categorized as
789 low and high based on the HOXA1 gene-set activation levels showed pyrimidine metabolic
790 process enrichment in high-HOXA1 categorized cell lines. Ranking of genes with
791 signal2noise metric was used for GSEA.
792 B. Gene-set enrichment analysis of KEGG pyrimidine metabolism gene-set in the gene
793 expression profile of cancer cell line encyclopedia (CCLE) panel (N = 917) categorized as
794 low and high based on the TNC gene-set activation levels showed pyrimidine metabolic
795 process enrichment in low-TNC categorized cell lines. Ranking of genes with signal2noise
796 metric was used for GSEA.
797 C. Schematic representation of TS gene-set derived from the RNA-seq expression profiling
798 of Calu-1 cells stably transduced with a lentiviral construct containing mCherry gene under
799 the control of *TYMS* promoter, and sorted the cells based on the low (5%) and high (5%)
800 *TYMS*-driven promoter activity.
801 D. Bar plot of correlation scores calculated between Calu-1 TS gene-set and the positive
802 (orange) or negative (blue) pathways of PyMet. **** - *P*-value < 0.0001; *** - *P*-value < 0.001;
803 ** - *P*-value < 0.01; ns – non-significant.
804 E. Schematic representation of TS gene-set derived from the RNA-seq expression profiling
805 of A549 cells knockdown for *TYMS* gene using stable shRNA lentiviral transduction.

806 F. Bar plot of correlation scores calculated between A549 TS gene-set and the positive
807 (orange) or negative (blue) pathways of PyMet. **** - *P*-value < 0.0001; *** - *P*-value < 0.001;
808 ** - *P*-value < 0.01; * - *P*-value < 0.05; ns – non-significant.
809 G. Bar plot of correlation scores calculated between PyMet and the positive (orange) or
810 negative (blue) pathways of PyMet in parental A549 cells sequenced using single cell RNA-
811 seq. **** - *P*-value < 0.0001; ns – non-significant.
812 H. Dot plot pattern analysis of positively associated signaling pathways of PyMet using
813 AddmoduleScore function in Seurat showed the enrichment of pyrimidine and its associated
814 pathways in cluster 1 of parental A549 cells from scRNA sequencing.
815
816 **Figure 3. RNA-seq expression profiling of brequinar (BRQ) treated cells validates the**
817 **pyrimidine associated pathways.**
818 A. Schematic representation of pyrimidine metabolic pathway and targeting of DHODH with
819 brequinar (BRQ).
820 B. Western blot analysis of TS protein levels in A549 cells treated with brequinar (BRQ) in
821 the indicated dose dependent concentration for 72 h. β-actin was used as an internal control.
822 C. Principal component analysis of RNA-seq expression profile of A549 cells treated with 1
823 μM of BRQ for 72 h reveals a high variance in the gene expression profiles between the
824 treated and the control samples (n = 3 per group).
825 D. Box plot visualization of the increased up-regulated gene-set of TNC signaling pathway
826 in the BRQ (1 μM) treated A549 cells compared to the control. The central band inside the
827 box represents the median value of the data (n = 3) obtained using the lower (bottom) and
828 upper (top) quartile values of the box. The maximum and minimum values of the data are

829 displayed with the vertical lines (whiskers) connecting the box. Significance was calculated
830 using un-paired *t*-test between the BRQ treatment and the control conditions.
831 E, F. Gene set enrichment analysis of down-regulated (E) and up-regulated (F) gene-sets
832 of HOXA1 signaling pathway in TCGA lung adenocarcinoma patient gene expression
833 profiles (N = 510) categorized as BRQ-high and BRQ-low based on the median of the BRQ
834 gene-set activation scores. Ranking of genes with signal2noise metric was used for GSEA.
835 G. Correlation matrix plot depicting the associations between BRQ gene-set, PyMet and its
836 associated signaling pathways in lung adenocarcinoma patients (N = 510).
837 H. Correlation values between BRQ gene-set and positively (or negatively) associated
838 pathways of PyMet calculated from the activation scores of the gene-sets in lung
839 adenocarcinoma patients (N = 510). **** - *P*-value < 0.0001; ns – non-significant.
840 I. Western blot analysis of TNC, DAX1 and TS protein levels in A549 cells treated with
841 brequinar (BRQ) in the indicated dose dependent concentration for 72 h. β-actin was used
842 as an internal control.
843 J. Western blot analysis of phosphorylated P53, TS and KRAS protein levels in A549 cells
844 treated with brequinar (BRQ) in the indicated dose dependent concentration for 72 h. β-actin
845 was used as an internal control.
846 K. Western blot analysis of phosphorylated mTOR, TS, TNC, DAX1 and P16 protein levels
847 in A549 cells knockdown for *TYMS* compared to the control (pLKO.1). β-actin was used as
848 an internal control.
849
850 **Figure 4. Pyrimidine metabolic process and its associated signaling pathways poses**
851 **chemoresistance in cancer.**

852 A. Correlation matrix plot depicting the associations between drug resistance gene-sets,
853 BRQ, pyrimidine and its associated signaling pathways in pancreatic adenocarcinoma (N =
854 177).
855 B. Scatter plots of the activation scores between doxorubicin drug resistance and pyrimidine
856 metabolism, its associated signaling pathways (HOXA1 and TNC) and BRQ gene-sets in
857 pancreatic adenocarcinoma (N = 177). Doxorubicin drug resistance showed positive
858 associations with pyrimidine and HOXA1, while negative associations were observed with
859 DHODH inhibitor (BRQ) and TNC signaling pathway.
860 C. Correlation matrix plot depicting the associations between drug resistance gene-sets,
861 BRQ, pyrimidine and its associated signaling pathways in lung adenocarcinoma (N = 510).
862 D. Scatter plots of the activation scores between doxorubicin drug resistance and pyrimidine
863 metabolism, its associated signaling pathways (HOXA1 and TNC) and BRQ gene-sets in
864 lung adenocarcinoma (N = 510). Doxorubicin drug resistance showed positive associations
865 with pyrimidine and HOXA1, while negative associations were observed with DHODH
866 inhibitor (BRQ) and TNC signaling pathway.
867 E. Gene set enrichment analysis of up-regulated gene-set of TNC signaling pathway in the
868 gene expression profile of IMR32 cell line treated with teriflunomide obtained from GEO
869 (GSE67338). Ranking of genes with signal2noise metric was used for GSEA.
870 F. Heatmap visualization of the rate-limiting genes of pyrimidine metabolism in the gene
871 expression profile of A549 cells resistant to cisplatin obtained from GEO (GSE108214).
872 G. Heatmap visualization of the rate-limiting genes of pyrimidine metabolism in the gene
873 expression profile of Calu-3 cells resistant to gemcitabine obtained from GEO (GSE6914).
874

875 **Figure 5. Pyrimidine pathway explorer (PYPE), a web resource for identifying the**
876 **associations of pyrimidine metabolic process.**
877 A. Schematic representation of the pipeline of pyrimidine pathway explorer (PYPE) to
878 analyze the user-defined gene-set and pyrimidine metabolism.
879 B,C. Identification of significant associations of Calu-1 TS gene-set (B) and A549 TS gene-
880 set (C) gene-sets with PyMet in a pan-cancer analysis using PYPE web tool.
881 D. Screenshot of PYPE web resource tool for performing pan-cancer analysis of pyrimidine
882 metabolism with signaling pathways and metabolic processes across 32 cancer types.
883
884 **Supplementary figure legends**
885 **Supplementary Figure S1. Pan-cancer transcriptome analysis has identified novel**
886 **connections of signaling pathways and metabolic processes with pyrimidine**
887 **metabolism.**
888 A-C. Correlation matrix plot of the top positively and negatively associated signaling
889 pathways of PyMet along with KEGG pyrimidine and REACTOME pyrimidine metabolism in
890 BRCA (N = 1082) (A), COAD (N = 592) (B) and UCEC (N = 527) (C) gene expression profiles
891 using pathway-based approach.
892 D. Heatmap visualization of correlation values between top positively and negatively
893 associated metabolic processes with PyMet across 32 cancer types.
894 E. Correlation plot depicting the negative association between the activation scores of
895 leucine deprivation and PyMet gene-sets in stomach adenocarcinoma gene expression
896 profile (N = 412).
897

898 **Supplementary Figure S2. Pyrimidine association with signaling pathways and**
899 **metabolic processes were recapitulated in CCLE and parental single cell RNA-**
900 **sequencing.**

901 A-C. Gene-set enrichment analysis of KEGG pyrimidine metabolism gene-set in the gene
902 expression profile of cancer cell line encyclopedia (CCLE) panel (N = 917) categorized as
903 low and high based on the ESRRA (A), FLI1-DAX1 (B) or SOX4 (C) gene-set activation
904 levels showed pyrimidine metabolic process enrichment in high-ESRRA (A) or high-FLI1
905 and DAX1 (B) categorized cell lines and in low-SOX4 (C) categorized cell lines. Ranking of
906 genes with signal2noise metric was used for GSEA.

907 D-F. Dot plot pattern analysis of negatively associated signaling pathways (D), positively
908 associated metabolic processes (E) and negatively associated metabolic processes (F) of
909 PyMet in the scRNA-seq of parental A549 cells. Percent expression and average expression
910 was estimated using AddmoduleScore function in Seurat.

911

912 **Supplementary Figure S3. RNA-seq expression profiling of BRQ treated samples**
913 **substantiate the pyrimidine associated pathways**

914 A. MA plot of differentially expressed genes identified in A549 cell line treated with BRQ for
915 72 h compared to the control (n = 3 per group). Blue dots represent the significantly
916 differentially expressed genes with a fold change of $\log_2$ (1).

917 B. Venn diagram representation of overlap analysis of the gene content between pyrimidine
918 metabolism genes and BRQ down-regulated genes. Significance was calculated using the
919 hypergeometric distribution method.

920 C,D. Enrichr based gene enrichment analysis of BRQ up-regulated genes in MSigDB gene-
921 sets collection (C), and BRQ down-regulated genes overlap with Bioplanet 2019 (D).

922 E-G. Box plot visualization of decreased activation levels of pyrimidine metabolism (E), and
923 FLI1-DAX1 down-regulated gene-set (F) in the RNA-seq samples of BRQ (1 μM) treated
924 A549 cells compared to the control. TP53 and TP73 target gene-sets were found expressed
925 with BRQ treatment (G). The central band inside the box represents the median value of the
926 data (n = 3) obtained using the lower (bottom) and upper (top) quartile values of the box.
927 The maximum and minimum values of the data are displayed with the vertical lines
928 (whiskers) connecting the box. Significance was calculated using un-paired *t*-test between
929 the BRQ treated cells and the control.
930 H,I. Gene set enrichment analysis of up-regulated gene-set of TNC signaling pathway (H)
931 and KEGG pyrimidine metabolism (I) in TCGA lung adenocarcinoma (N = 510) patients
932 categorized as BRQ-high and BRQ-low based on the median of BRQ gene-set activation
933 scores. Ranking of genes with signal2noise metric was used for GSEA.
934 J. Western blot analysis of TNC and TS protein levels in SKMES1 cells treated with
935 brequinar (BRQ) in the indicated dose-dependent manner for 48 h. β-actin was used as an
936 internal control.
937 K. Western blot analysis of DAX1 and TS protein levels in SKMES1 cells treated with
938 brequinar (BRQ) in the indicated dose-dependent manner for 72 h. β-actin was used as an
939 internal control.
940 L. Scatter plot of activation scores of KRAS and BRQ gene-sets in lung adenocarcinoma
941 patient samples (N = 510) showed a negative association pattern between KRAS and
942 DHODH inhibitor, BRQ.
943
944 **Supplementary Figure S4. Pyrimidine metabolic process and its associated signaling**
945 **pathways pose drug resistance in pan-cancer analysis.**

946 A. Correlation matrix plot depicting the associations between drug resistance gene-sets,
947 BRQ, pyrimidine and its associated signaling pathways in bladder carcinoma (N = 407).
948 B. Scatter plots of the activation scores between doxorubicin drug resistance and pyrimidine
949 metabolism, its associated signaling pathways (HOXA1 and TNC) and BRQ gene-sets in
950 bladder carcinoma (N = 407). Doxorubicin drug resistance showed positive associations with
951 pyrimidine and HOXA1, while negative associations were observed with DHODH inhibitor
952 (BRQ) and TNC signaling pathway.
953 C. Correlation matrix plot depicting the associations between drug resistance gene-sets,
954 BRQ, pyrimidine and its associated signaling pathways in breast invasive carcinoma (N =
955 1082).
956 D. Scatter plots of the activation scores between doxorubicin drug resistance and pyrimidine
957 metabolism, its associated signaling pathways (HOXA1 and TNC) and BRQ gene-sets in
958 breast invasive carcinoma (N = 1082). Doxorubicin drug resistance showed positive
959 associations with pyrimidine and HOXA1, while negative associations were observed with
960 DHODH inhibitor (BRQ) and TNC signaling pathway.
961 E. Correlation matrix plot depicting the associations between drug resistance gene-sets,
962 BRQ, pyrimidine and its associated signaling pathways in low grade glioma (N = 514).
963 F. Scatter plots of the activation scores between doxorubicin drug resistance and pyrimidine
964 metabolism, its associated signaling pathways (HOXA1 and TNC) and BRQ gene-sets in
965 low grade glioma (N = 514). Doxorubicin drug resistance showed positive associations with
966 pyrimidine and HOXA1, while negative associations were observed with DHODH inhibitor
967 (BRQ) and TNC signaling pathway.

Figure 1

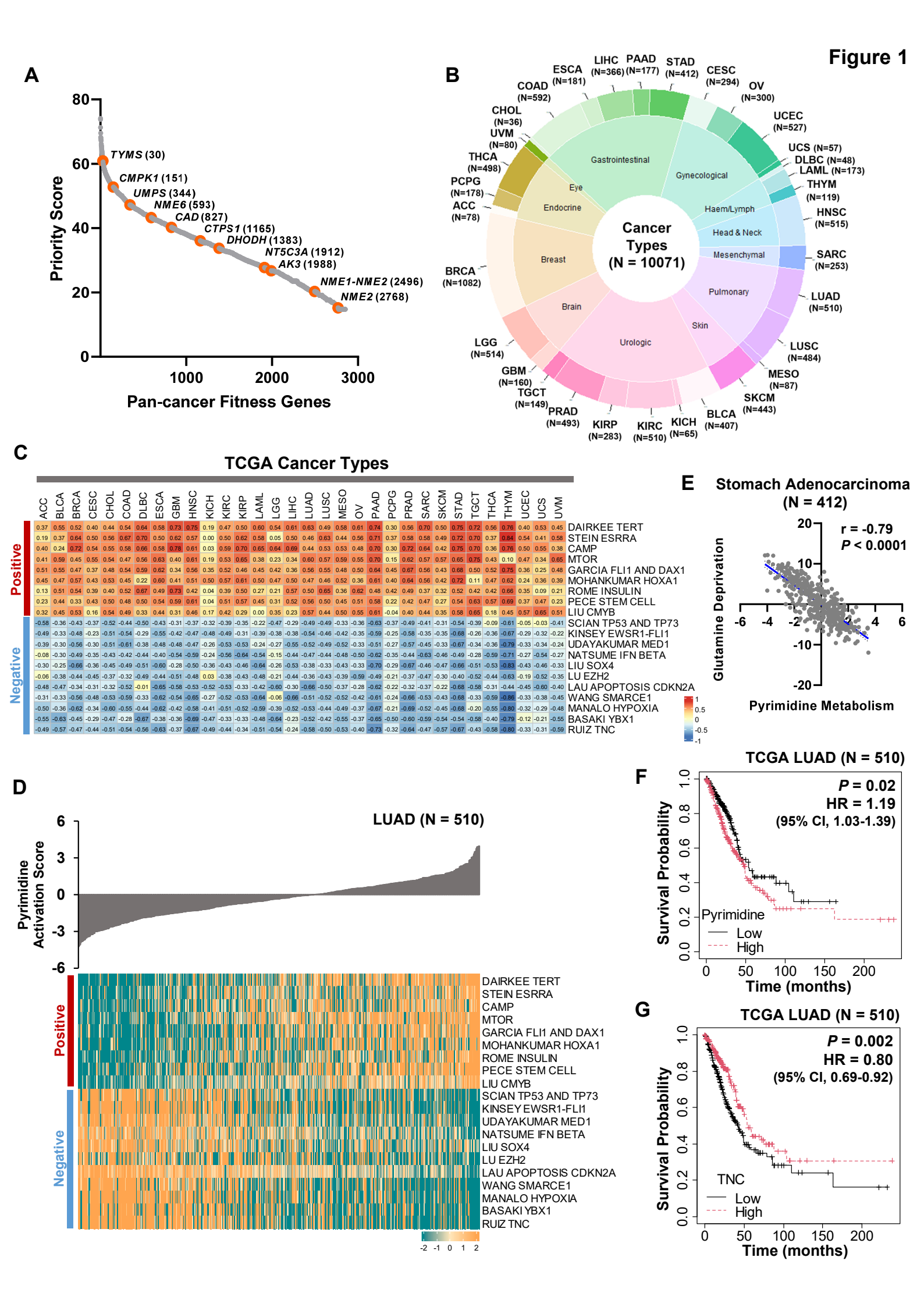
A
Priority Score
Pan-cancer Fitness Genes
TYMS (30)
CMPK1 (151)
UMPS (344)
NME6 (593)
CAD (827)
CTPS1 (1165)
DHODH (1383)
NT5C3A (1912)
AK3 (1988)
NME1-NME2 (2496)
NME2 (2768)
B
Cancer Types (N = 10071)
Gastrointestinal
Gynecological
Haem/Lymph
Head & Neck
Mesenchymal
Pulmonary
Skin
Urologic
Brain
Breast
Endocrine
Eye
ESCA (N=181)
LIHC (N=366)
PAAD (N=177)
STAD (N=412)
CESC (N=294)
OV (N=300)
UCEC (N=527)
UCS (N=57)
DLBC (N=48)
LAML (N=173)
THYM (N=119)
HNSC (N=515)
SARC (N=253)
LUAD (N=510)
LUSC (N=484)
MESO (N=87)
SKCM (N=443)
BLCA (N=407)
KICH (N=65)
KIRC (N=510)
KIRP (N=283)
PRAD (N=493)
TGCT (N=149)
GBM (N=160)
LGG (N=514)
BRCA (N=1082)
ACC (N=78)
PCPG (N=178)
THCA (N=498)
UVM (N=80)
CHOL (N=36)
COAD (N=592)
C
TCGA Cancer Types
Positive
Negative
DAIRKEE TERT
STEIN ESRRA
CAMP
MTOR
GARCIA FLI1 AND DAX1
MOHANKUMAR HOXA1
ROME INSULIN
PECE STEM CELL
LIU CMYB
SCIAN TP53 AND TP73
KINSEY EWSR1-FLI1
UDAYAKUMAR MED1
NATSUME IFN BETA
LIU SOX4
LU EZH2
LAU APOPTOSIS CDKN2A
WANG SMARCE1
MANALO HYPOXIA
BASAKI YBX1
RUIZ TNC
E
Stomach Adenocarcinoma (N = 412)
r = -0.79
P < 0.0001
Glutamine Deprivation
Pyrimidine Metabolism
D
LUAD (N = 510)
Pyrimidine Activation Score
Positive
Negative
F
TCGA LUAD (N = 510)
P = 0.02
HR = 1.19
(95% CI, 1.03-1.39)
Survival Probability
Pyrimidine
Low
High
Time (months)
G
TCGA LUAD (N = 510)
P = 0.002
HR = 0.80
(95% CI, 0.69-0.92)
Survival Probability
TNC
Low
High
Time (months)

Figure 2

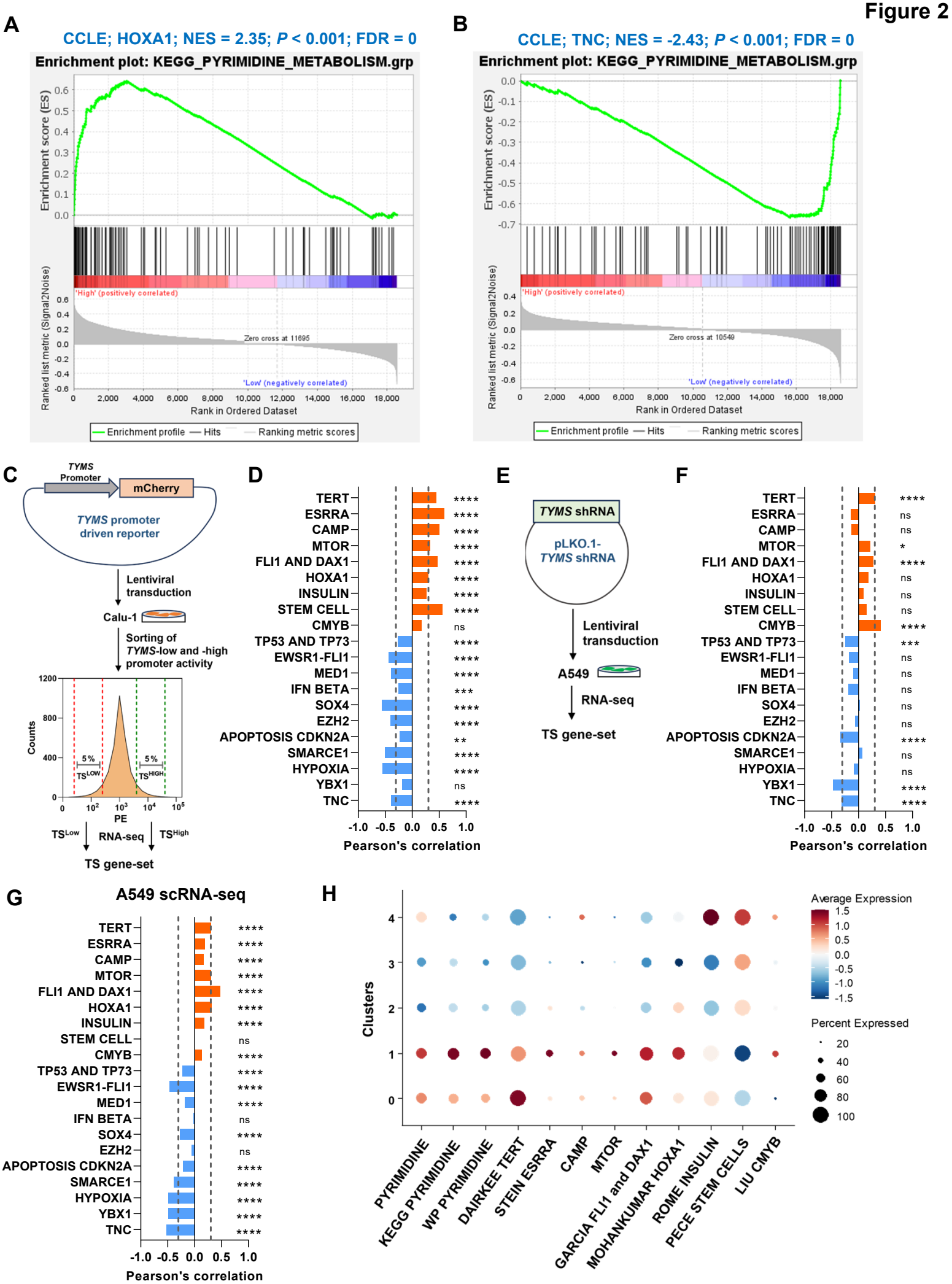
A
CCLE; HOXA1; NES = 2.35; P < 0.001; FDR = 0
Enrichment plot: KEGG_PYRIMIDINE_METABOLISM.grp
Enrichment score (ES)
'High' (positively correlated)
Zero cross at 11695
'Low' (negatively correlated)
Ranked list metric (Signal2Noise)
Rank in Ordered Dataset
Enrichment profile
Hits
Ranking metric scores
B
CCLE; TNC; NES = -2.43; P < 0.001; FDR = 0
Enrichment plot: KEGG_PYRIMIDINE_METABOLISM.grp
Zero cross at 10549
C
TYMS Promoter
mCherry
TYMS promoter driven reporter
Lentiviral transduction
Calu-1
Sorting of TYMS-low and -high promoter activity
Counts
PE
TSLow
RNA-seq
TSHigh
TS gene-set
D
TERT
ESRRA
CAMP
MTOR
FLI1 AND DAX1
HOXA1
INSULIN
STEM CELL
CMYB
TP53 AND TP73
EWSR1-FLI1
MED1
IFN BETA
SOX4
EZH2
APOPTOSIS CDKN2A
SMARCE1
HYPOXIA
YBX1
TNC
Pearson's correlation
E
TYMS shRNA
pLKO.1-TYMS shRNA
Lentiviral transduction
A549
RNA-seq
TS gene-set
F
Pearson's correlation
G
A549 scRNA-seq
Pearson's correlation
H
Clusters
Average Expression
Percent Expressed
PYRIMIDINE
KEGG PYRIMIDINE
WP PYRIMIDINE
DAIRKEE TERT
STEIN ESRRA
CAMP
MTOR
GARCIA FLI1 and DAX1
MOHANKUMAR HOXA1
ROME INSULIN
PECE STEM CELLS
LIU CMYB

Figure 3

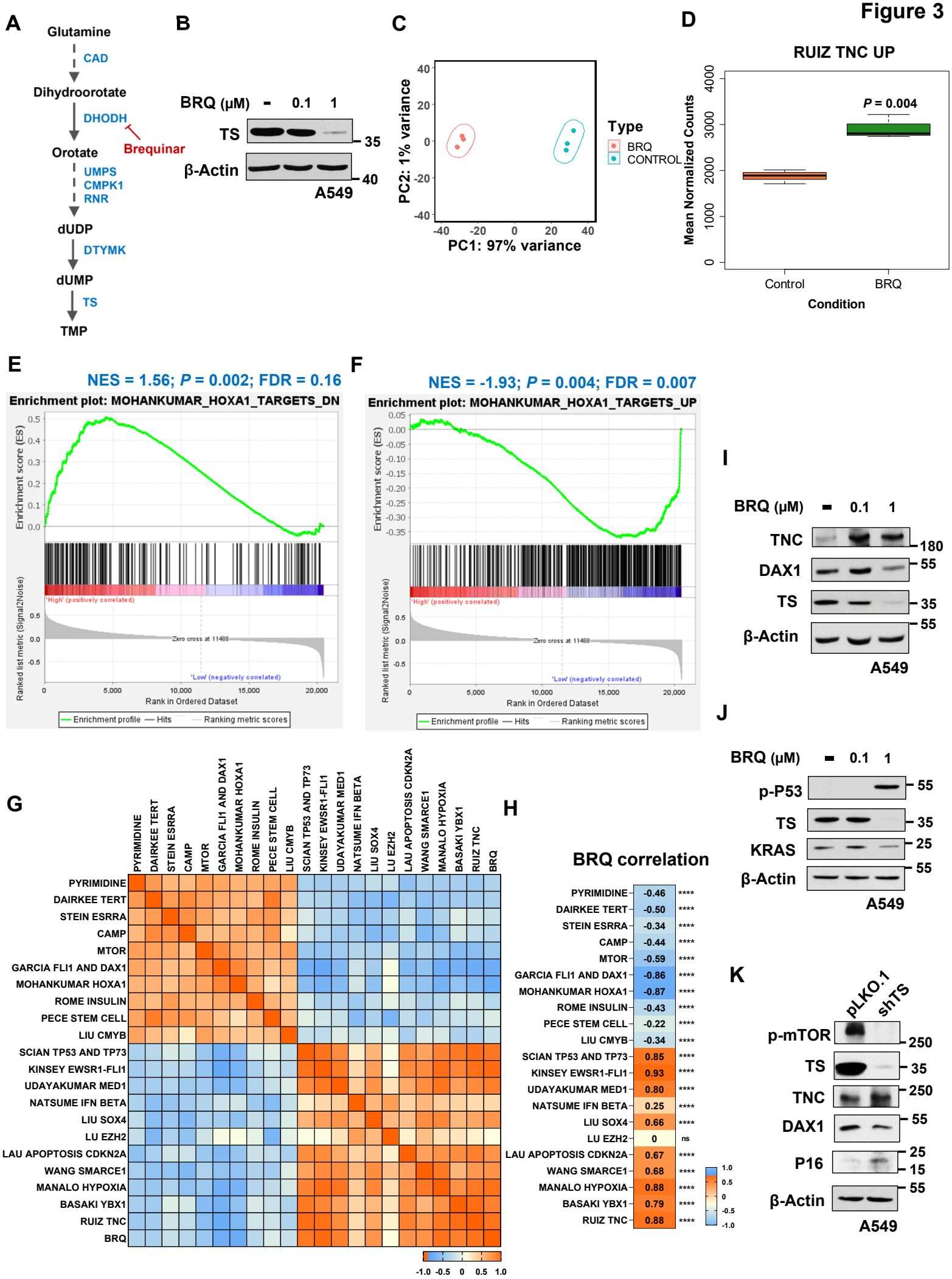
A
Glutamine
CAD
Dihydroorotate
DHODH
Brequinar
Orotate
UMPS
CMPK1
RNR
dUDP
DTYMK
dUMP
TS
TMP
B
BRQ (μM) - 0.1 1
TS
β-Actin
35
40
A549
C
PC2: 1% variance
PC1: 97% variance
Type
BRQ
CONTROL
D
RUIZ TNC UP
P = 0.004
Mean Normalized Counts
Control
BRQ
Condition
E
NES = 1.56; P = 0.002; FDR = 0.16
Enrichment plot: MOHANKUMAR_HOXA1_TARGETS_DN
Enrichment score (ES)
'High' (positively correlated)
Zero cross at 11488
'Low' (negatively correlated)
Ranked list metric (Signal2Noise)
Rank in Ordered Dataset
Enrichment profile
Hits
Ranking metric scores
F
NES = -1.93; P = 0.004; FDR = 0.007
Enrichment plot: MOHANKUMAR_HOXA1_TARGETS_UP
Enrichment score (ES)
'High' (positively correlated)
Zero cross at 11488
'Low' (negatively correlated)
Ranked list metric (Signal2Noise)
Rank in Ordered Dataset
Enrichment profile
Hits
Ranking metric scores
I
BRQ (μM) - 0.1 1
TNC
DAX1
TS
β-Actin
180
55
35
55
A549
J
BRQ (μM) - 0.1 1
p-P53
TS
KRAS
β-Actin
55
35
25
55
A549
G
PYRIMIDINE
DAIRKEE TERT
STEIN ESRRA
CAMP
MTOR
GARCIA FLI1 AND DAX1
MOHANKUMAR HOXA1
ROME INSULIN
PECE STEM CELL
LIU CMYB
SCIAN TP53 AND TP73
KINSEY EWSR1-FLI1
UDAYAKUMAR MED1
NATSUME IFN BETA
LIU SOX4
LU EZH2
LAU APOPTOSIS CDKN2A
WANG SMARCE1
MANALO HYPOXIA
BASAKI YBX1
RUIZ TNC
BRQ
-1.0 -0.5 0 0.5 1.0
H
BRQ correlation
PYRIMIDINE -0.46 ****
DAIRKEE TERT -0.50 ****
STEIN ESRRA -0.34 ****
CAMP -0.44 ****
MTOR -0.59 ****
GARCIA FLI1 AND DAX1 -0.86 ****
MOHANKUMAR HOXA1 -0.87 ****
ROME INSULIN -0.43 ****
PECE STEM CELL -0.22 ****
LIU CMYB -0.34 ****
SCIAN TP53 AND TP73 0.85 ****
KINSEY EWSR1-FLI1 0.93 ****
UDAYAKUMAR MED1 0.80 ****
NATSUME IFN BETA 0.25 ****
LIU SOX4 0.66 ****
LU EZH2 0 ns
LAU APOPTOSIS CDKN2A 0.67 ****
WANG SMARCE1 0.68 ****
MANALO HYPOXIA 0.88 ****
BASAKI YBX1 0.79 ****
RUIZ TNC 0.88 ****
1.0
0.5
0
-0.5
-1.0
K
pLKO.1
shTS
p-mTOR
TS
TNC
DAX1
P16
β-Actin
250
35
250
55
25
15
55
A549

Figure 4

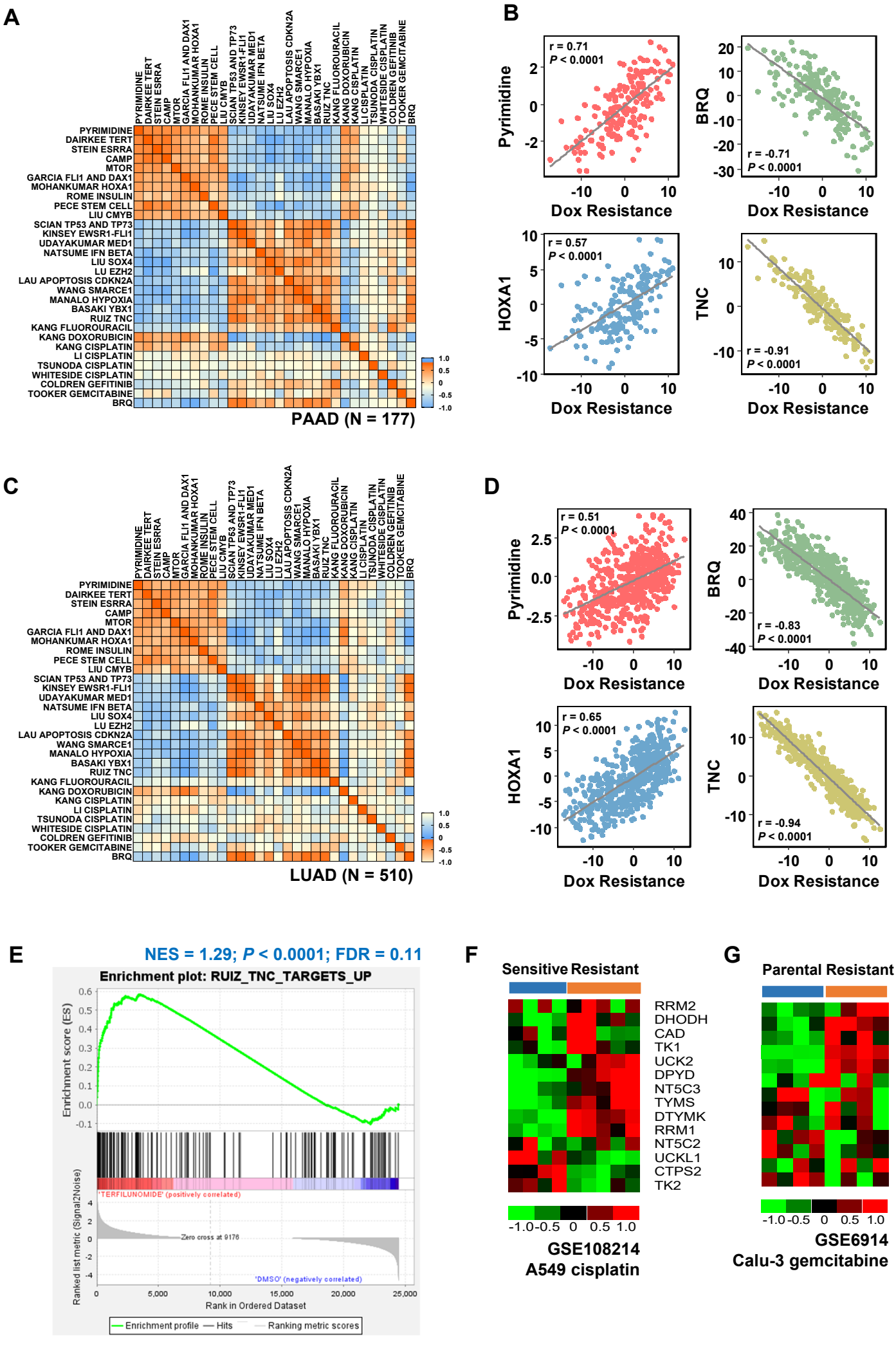
A
PAAD (N = 177)
B
r = 0.71
P < 0.0001
r = -0.71
P < 0.0001
r = 0.57
P < 0.0001
r = -0.91
P < 0.0001
Pyrimidine
BRQ
HOXA1
TNC
Dox Resistance
C
LUAD (N = 510)
D
r = 0.51
P < 0.0001
r = -0.83
P < 0.0001
r = 0.65
P < 0.0001
r = -0.94
P < 0.0001
E
NES = 1.29; P < 0.0001; FDR = 0.11
Enrichment plot: RUIZ_TNC_TARGETS_UP
Enrichment score (ES)
'TERFILUNOMIDE' (positively correlated)
Zero cross at 9176
'DMSO' (negatively correlated)
Ranked list metric (Signal2Noise)
Rank in Ordered Dataset
Enrichment profile
Hits
Ranking metric scores
F
Sensitive Resistant
RRM2
DHODH
CAD
TK1
UCK2
DPYD
NT5C3
TYMS
DTYMK
RRM1
NT5C2
UCKL1
CTPS2
TK2
GSE108214
A549 cisplatin
G
Parental Resistant
TYMS
CAD
DHODH
RRM1
UCK2
TK2
DTYMK
CTPS1
TK1
CTPS2
UCKL1
NT5C2
RRM2
GSE6914
Calu-3 gemcitabine

Figure 5

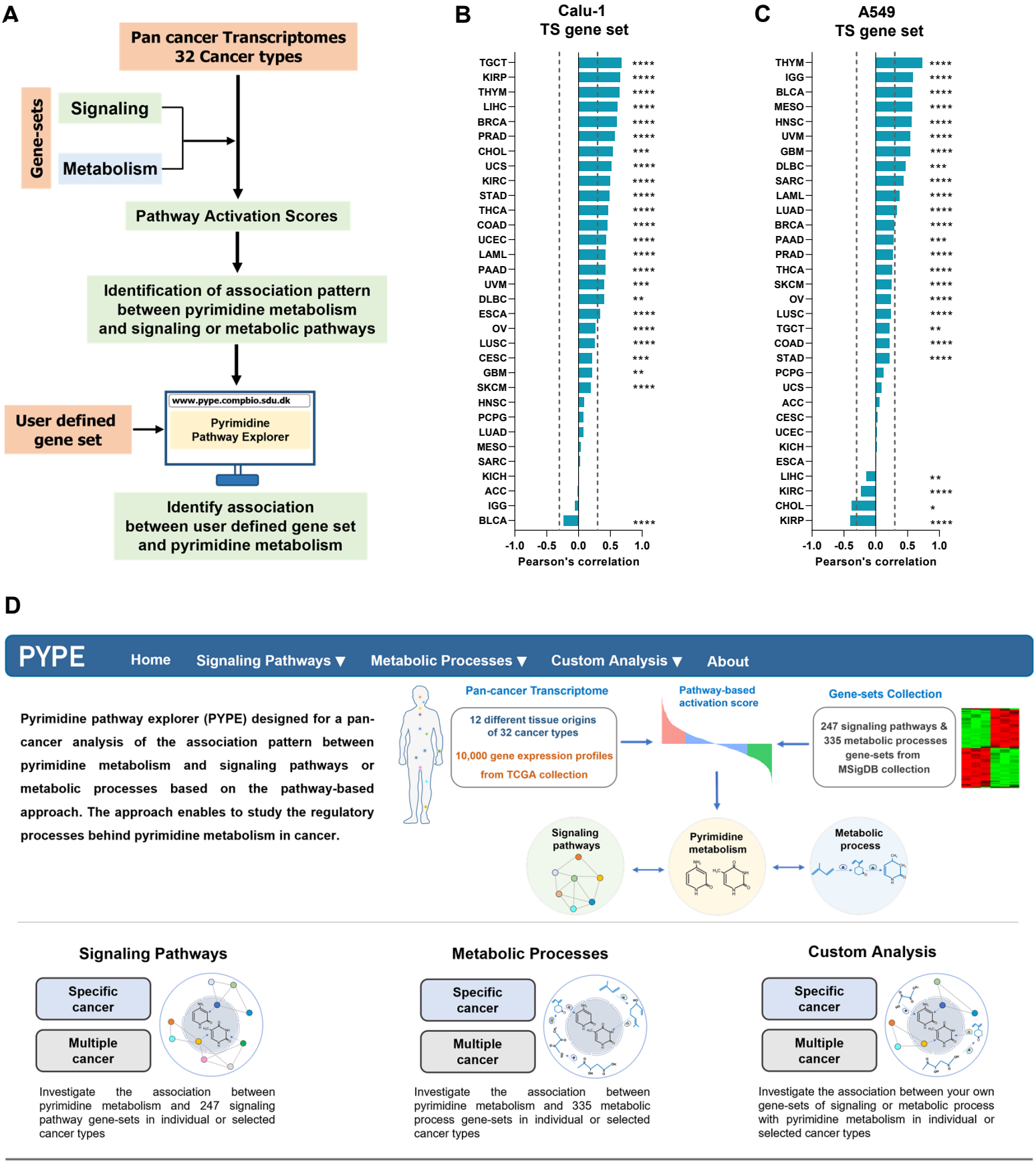
A
Pan cancer Transcriptomes
32 Cancer types
Gene-sets
Signaling
Metabolism
Pathway Activation Scores
Identification of association pattern between pyrimidine metabolism and signaling or metabolic pathways
User defined gene set
www.pype.compbio.sdu.dk
Pyrimidine Pathway Explorer
Identify association between user defined gene set and pyrimidine metabolism
B
Calu-1
TS gene set
TGCT KIRP THYM LIHC BRCA PRAD CHOL UCS KIRC STAD THCA COAD UCEC LAML PAAD UVM DLBC ESCA OV LUSC CESC GBM SKCM HNSC PCPG LUAD MESO SARC KICH ACC IGG BLCA
-1.0 -0.5 0.0 0.5 1.0
Pearson's correlation
C
A549
TS gene set
THYM IGG BLCA MESO HNSC UVM GBM DLBC SARC LAML LUAD BRCA PAAD PRAD THCA SKCM OV LUSC TGCT COAD STAD PCPG UCS ACC CESC UCEC KICH ESCA LIHC KIRC CHOL KIRP
-1.0 -0.5 0.0 0.5 1.0
Pearson's correlation
D
PYPE
Home
Signaling Pathways
Metabolic Processes
Custom Analysis
About
Pyrimidine pathway explorer (PYPE) designed for a pan-cancer analysis of the association pattern between pyrimidine metabolism and signaling pathways or metabolic processes based on the pathway-based approach. The approach enables to study the regulatory processes behind pyrimidine metabolism in cancer.
Pan-cancer Transcriptome
12 different tissue origins of 32 cancer types
10,000 gene expression profiles from TCGA collection
Pathway-based activation score
Gene-sets Collection
247 signaling pathways & 335 metabolic processes gene-sets from MSigDB collection
Signaling pathways
Pyrimidine metabolism
Metabolic process
Signaling Pathways
Specific cancer
Multiple cancer
Investigate the association between pyrimidine metabolism and 247 signaling pathway gene-sets in individual or selected cancer types
Metabolic Processes
Specific cancer
Multiple cancer
Investigate the association between pyrimidine metabolism and 335 metabolic process gene-sets in individual or selected cancer types
Custom Analysis
Specific cancer
Multiple cancer
Investigate the association between your own gene-sets of signaling or metabolic process with pyrimidine metabolism in individual or selected cancer types